TASK QUARTERLY 16 No 1, 75–96

STUDY OF ICOSAHEDRAL CLUSTERS IN CLOSE-PACKED SIMPLE LIQUIDS

AGNIESZKA L. KOZUB

Faculty of Applied Physics and Mathematics,
Gdansk University of Technology,
Narutowicza 11/12, 80-233 Gdansk, Poland
aga.kozub@gmail.com

(Received 5 October 2011; revised manuscript received 20 December 2011)

Abstract: The local structure of liquid copper was determined using Steinhardt order parameters, with particular attention paid to icosahedral clusters. The positions of atoms were obtained from three sets of molecular dynamics simulations, with the forces obtained from: the Sutton-Chen (SC) potential, the Naval Research Laboratory total energy tight-binding (NRL-TB) method and the divide-and-conquer learn-on-the-fly (DCLOTF) method, respectively. A broad range of local geometries appeared, which is a typical result for close-packed liquids. Among them a number of icosahedral clusters were detected. The highest density of icosahedral clusters was obtained at the temperature of 1000K for the NRL-TB and DCLOTF simulations and 1200K for the SC simulations. I propose various means of analysing the icosahedral clusters formed in liquid copper. The average number of the clusters, their lifetime and correlations between them at various temperatures were studied as a function of the approach used to generate the trajectories. Finally, I studied the formation and decay of icosahedral clusters.

Keywords: liquid metals, icosahedral clusters, structure, molecular-dynamics

1. Introduction

Liquid copper is a typical example of a close-packed liquid metal, with the atoms lacking any long-range periodic order. As a close-packed liquid, it is characterised by a broad range of local geometries, among them also icosahedral clusters.

A 13-atom icosahedral cluster is composed of twelve atoms symmetrically placed around the central atom, forming twenty identical tetrahedra, with atoms placed in the vertices. Since it possesses a five-fold rotational symmetry, it is not packed perfectly. Moreover, due to this property, icosahedral clusters do not form periodic crystals [1].

Icosahedral clusters appearing in liquid metals were the subject of many studies, both theoretical and experimental. The interest in the topic increased

after 1952, when Frank [2] noticed that, at least in the case of the Lennard-Jones potential, icosahedral clustering is more favourable than other possible 13-atom configurations, *i.e.* face-centred cubic (*fcc*) and hexagonal close-packed (*hcp*) clusters. The structure of the icosahedron has notably lower energy than both of the *fcc* and *hcp* clusters [2].

A widely used approach for analysing the structure of matter in molecular simulations was proposed thirty years after Frank's publication by Steinhardt, Nelson and Ronchetti [3]. Their algorithm involves calculating so-called local bond order parameters (BOPs) also known as Steinhardt order parameters. It is based on quadratic and third-order invariants defined by spherical harmonics related to bonds between an atom and its neighbours, where the "bond" term refers to the line segment connecting two atoms. They are defined as:

$$Q_l = \sqrt{\frac{4\pi}{2l+1}\sum_{m=-l}^{m=l}|\overline{Q}_{lm}|^2} \tag{1}$$

$$\widehat{W}_l = \frac{\sum\limits_{\substack{m_1,m_2,m_3 \\ m_1+m_2+m_3=0}} \begin{pmatrix} l & l & l \\ m_1 & m_2 & m_3 \end{pmatrix} \overline{Q}_{lm_1}\overline{Q}_{lm_2}\overline{Q}_{lm_3}}{\left(\sum\limits_{m=-l}^{l}|\overline{Q}_{lm}|^2\right)^{\frac{3}{2}}} \tag{2}$$

where:

$$\overline{Q}_{lm} = \frac{1}{N_b}\sum_{j=1}^{N_b} Y_{lm}(\theta(\vec{r}),\phi(\vec{r})) \tag{3}$$

The vector $\vec{r}$ corresponds to the midpoint of the bond connecting the two atoms; $\theta(\vec{r})$ and $\phi(\vec{r})$ are the polar angles of this bond measured with respect to the fixed reference frame; $Y_{lm}(\theta,\phi)$ are spherical harmonics of degree l and order m (where $-l \le m \le l$); N_b is the set of the nearest neighbours of the considered atom; m_1, m_2 and m_3 are integers ranging from $-l$ to l and the coefficients $\begin{pmatrix} l & l & l \\ m_1 & m_2 & m_3 \end{pmatrix}$ are the so-called Wigner $3j$ symbols [4].

The choice of the index l has a significant role in the analysis. Only BOPs with even values of l are taken into consideration, since the parameters should be invariant to the interchange of particles. Each of the parameters can be used to detect a different kind of symmetry. BOPs with indices $l=4$ and $l=6$ are often used, as they effectively distinguish cubic and hexagonal structures [5].

Icosahedral clusters were detected experimentally in liquid copper, using X-ray absorption spectroscopy [6, 7]. The study was performed at the temperatures of 1313K, 1398K and 1623K. According to the experimental results, about 10% of local structures in liquid copper could be classified as nearly-icosahedral. Such a small fraction was suggested to be typical for close-packed liquid metals since the excluded volume effect has a significant impact on structure of such materials [8].

The main aim of this work was to study icosahedral clusters appearing in computer-simulated liquid copper, their concentration and average lifetime as a function of the temperature for which calculations were performed. I also analysed the correlations between icosahedral clusters and the concentration of incomplete icosahedral clusters with one, two or three atoms removed from the outer shell. Finally, the mechanisms of formation and decay of icosahedral clusters were studied.

2. Simulation details

2.1. Simulation parameters

The computer simulations used in this work were performed by Dziedzic [9]. A system consisting of 500 copper atoms was computer-simulated with the use of the molecular-dynamics method with three various approaches used to generate the forces driving the atoms: the semi-empirical, many-body Sutton-Chen potential [10], the Naval Research Laboratory total energy tight-binding method – an example of an electronic band-structure method [11–14] and the hybrid, quantum-classical divide-and-conquer learn-on-the-fly method [15, 16].

The atoms were subjected to periodic boundary conditions in all cases. Calculations were performed for ten temperatures between 1000 K and 1900 K in increments of 100 K. In all runs the timestep was equal to 0.5 fs and the positions were saved every 100 frames, *i.e.* every 50 fs. The frames corresponding to the equilibration period were discarded. The simulations were performed with the Nosé-Hoover thermostat and sampled the NVT ensemble. The cut-off radius in all cases was equal to 9 Å. The size of the simulation cell corresponded to the experimental volume of liquid copper at each temperature, taken from [17]. The parameters for the Sutton-Chen potential were fitted to copper in normal conditions.

2.2. The Sutton-Chen potential

The semi-empirical, many-body Sutton-Chen (SC) potential was designed for modelling *fcc* metals. Sutton and Chen [10] proposed a method which combines a many-body Finnis-Sinclair potential with the Lennard-Jones pair potential. For that reason the SC potential is able to model both the short-range interactions and the long-range van der Waals interactions. In its general form it can be written as:

$$U = \epsilon \left(\frac{1}{2} \sum_{\substack{i,j=1 \\ i \neq j}}^{N} U_2(r_{ij}) - C \sum_{i=1}^{N} \sqrt{\rho_i} \right) \tag{4}$$

where N denotes the number of particles within the cut-off radius, $r_{ij} = |\vec{r}_i - \vec{r}_j|$ is the distance between particles i and j, $U_2(r_{ij})$ is a two-body potential in the form of:

$$U_2(r_{ij}) = \left(\frac{a}{r_{ij}} \right)^n \tag{5}$$

and ρ_i is the local electron density:

$$\rho_i = \sum_{\substack{j=1 \\ j\neq i}}^{N} \left(\frac{a}{r_{ij}}\right)^m \tag{6}$$

The parameter a is close to the equilibrium lattice parameter, ϵ and C are determined by the lattice energies of the *fcc* lattice, the exponents m and n are integers satisfying $n > m$. They are chosen for the best modelling of the metal by fitting to elastic constants.

2.3. The Naval Research Laboratory total energy tight-binding approach

The Naval Research Laboratory total energy tight-binding approach (NRL-TB) [12, 13] is a variant of the quantum tight-binding (TB) method proposed by Slater and Koster [11]. Tight-binding methods, including the NRL-TB variant, are derived from the Schrödinger equation:

$$\hat{H}|\Psi_n\rangle = \varepsilon_n|\Psi_n\rangle \tag{7}$$

under the Born-Oppenheimer and one-electron approximations. In the above, $\hat{H}$ is the one-electron Hamiltonian operator, ε_n is the n^{th} electronic eigenlevel and $|\Psi_n\rangle$ is the corresponding eigenfunction of $\hat{H}$. The wave functions $|\Psi_n\rangle$ are obtained as a linear combination of atomic orbitals (the index i denotes the atom number and α indexes the atom's orbitals):

$$|\Psi_n\rangle = \sum_{i,\alpha} c^n_{i\alpha}|\phi_{i\alpha}\rangle \tag{8}$$

The Hamiltonian matrix is subsequently introduced:

$$\mathcal{H}_{i\alpha,j\beta} = \langle\phi_{i\alpha}|\hat{H}|\phi_{j\beta}\rangle \tag{9}$$

where j indexes atoms and β indexes orbitals.

The above equation can be transformed into an eigenvalue problem:

$$\mathcal{H}\mathcal{C} = \varepsilon\mathcal{C} \tag{10}$$

where the matrix $\mathcal{C}$ represents the electronic eigenvectors and ε represents the eigenvalues. Since the basis functions $|\phi_{i\alpha}\rangle$ may not be orthogonal in various variants of the TB approach (and in the NRL-TB variant in particular), the eigenvalue problem is often replaced by a generalised eigenvalue problem:

$$\mathcal{H}\mathcal{C} = \varepsilon\mathcal{S}\mathcal{C} \tag{11}$$

where $\mathcal{S}$ is an appropriate overlap matrix. To solve the eigenvalue problem several assumptions are undertaken [12, 18].

In the NRL-TB variant, the parameters involved in the functions that constitute the elements of the Hamiltonian matrix $\mathcal{H}$ and the overlap matrix S are obtained from a least-square minimisation involving the energy eigenvalues. They

approximate energy eigenvalues obtained from more accurate first-principles calculations, *e.g.* the full-potential Linearized Augmented Plane Wave method [14]. A particular feature of the NRL-TB variant is that the total energy of the system, which is obtained by shifting the Kohn-Sham energy levels, is also included in the fitting procedure.

2.4. The divide-and-conquer learn-on-the-fly approach

The hybrid quantum-classical divide-and-conquer learn-on-the-fly (DCLOTF) scheme is an extension of the learn-on-the-fly (LOTF) approach [16], where the accurate forces obtained from a first-principles approach are used to periodically, locally re-parametrise the classical potential by fitting the classical forces to the quantum-based forces. The least-squares difference between the two forces, calculated over the entire system, is used as the goal function in the fitting. Since the Sutton-Chen potential is many-body and is moderately long-ranged, the original approach runs into problems related to minimising a function of hundreds or thousands of variables. The DCLOTF extension works around this limitation by performing a series of local minimisations, over so-called grains, hoping to achieve global force-matching. The reader is referred to [15] for a more detailed description.

3. Technical results

3.1. The cut-off radius

The cut-off radius used to calculate the BOPs was set to a value ensuring that all atoms from the first coordination shell were included in the calculations. This is defined as all the atoms located no further than $1.2r_0$, where r_0 is the position of the first maximum in the radial distribution function (RDF). Figure 1 shows RDFs obtained for simulations performed with the use of the SC, NRL-TB and DCLOTF approaches. For NRL-TB and DCLOTF at all studied temperatures and for SC at the temperatures of 1200K and higher the position of the first peak was close to $r_0 = 2.5\,\text{Å}$. That gave a cut-off radius $r_{\text{cut}}^{\text{BOP}}$ equal to:

$$r_{\text{cut}}^{\text{BOP}} = 1.2r_0 = 3\,\text{Å} \tag{12}$$

For the SC simulations at the temperatures of 1000K and 1100K the values of r_0 and thus $r_{\text{cut}}^{\text{BOP}}$ were slightly larger, although I found it sufficient to consider their $r_{\text{cut}}^{\text{BOP}}$ to be also equal to 3Å.

3.2. The criteria for recognising 13-atom clusters

The recognition of structures appearing in the simulations was performed in two steps: first, by identifying atoms with twelve nearest neighbours and afterwards by calculating BOPs with indices $l = 4$ and $l = 6$. The calculations were performed with a C++ computer program written by Winczewski [19] in accordance with the method presented in Section 1. I found it useful to consider the structures with shapes similar to icosahedral, *fcc* or *hcp* clusters, where the

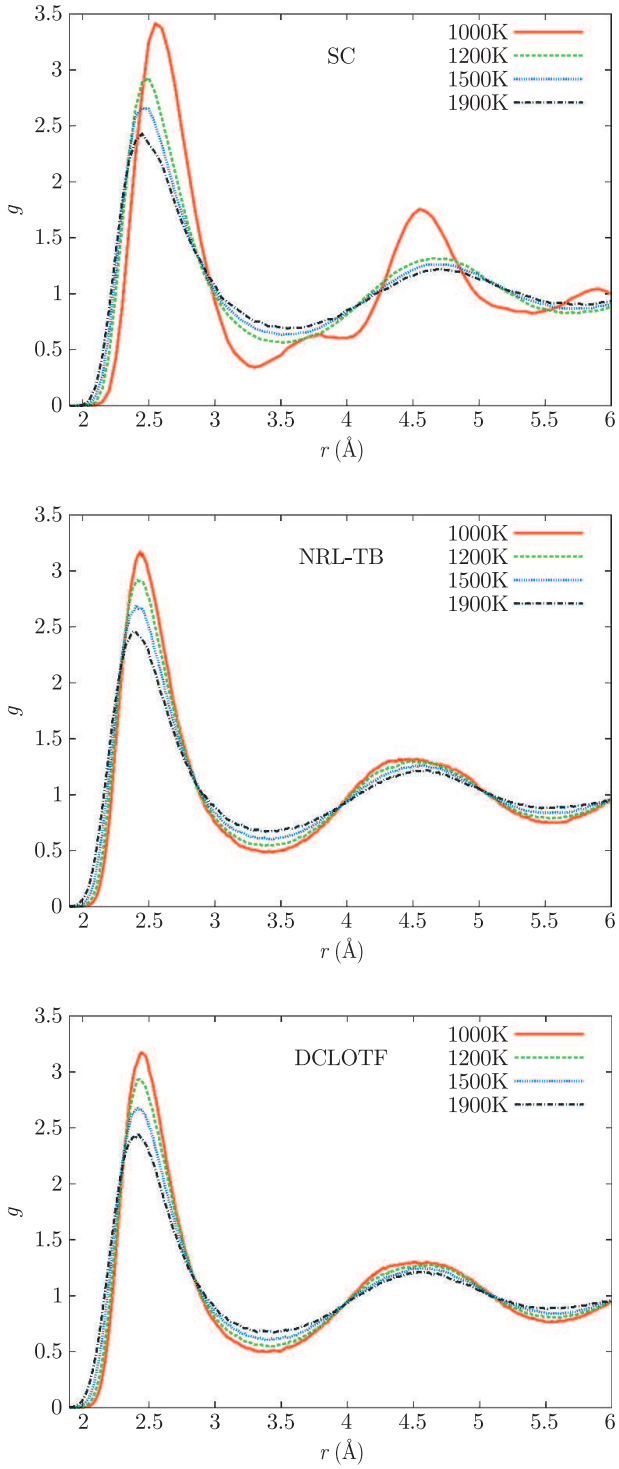

Figure 1. Radial distribution functions used to determine $r_{\mathrm{cut}}^{\mathrm{BOP}}$

positions of atoms were disturbed by no more than 5% of the bond length from the model structures. The magnitude and direction of the displacement were selected randomly from a Gaussian distribution.

The way BOPs are defined made it sufficient to verify just two of them, one from each group: Q_4 or $\widehat{W}_4$ and Q_6 or $\widehat{W}_6$. What follows from its definition $\widehat{W}_4$ is a poor choice for recognizing icosahedral clusters. The decision which of the remaining possibilities should be selected was made with the use of Figure 2. This scatter plots present the values of invariants $Q_4 - Q_6$ and $Q_4 - \widehat{W}_6$ of the central atom of a cluster, calculated for 10 000 examples of icosahedral-like, *fcc*-like and *hcp*-like clusters. For $Q_4 - \widehat{W}_6$ parameters one observes clearly separated islands corresponding to the icosahedral-like structures. In the scatter plots of $Q_4 - Q_6$ parameters the values of all three kinds of structures overlap. Therefore, they were not used in further investigations.

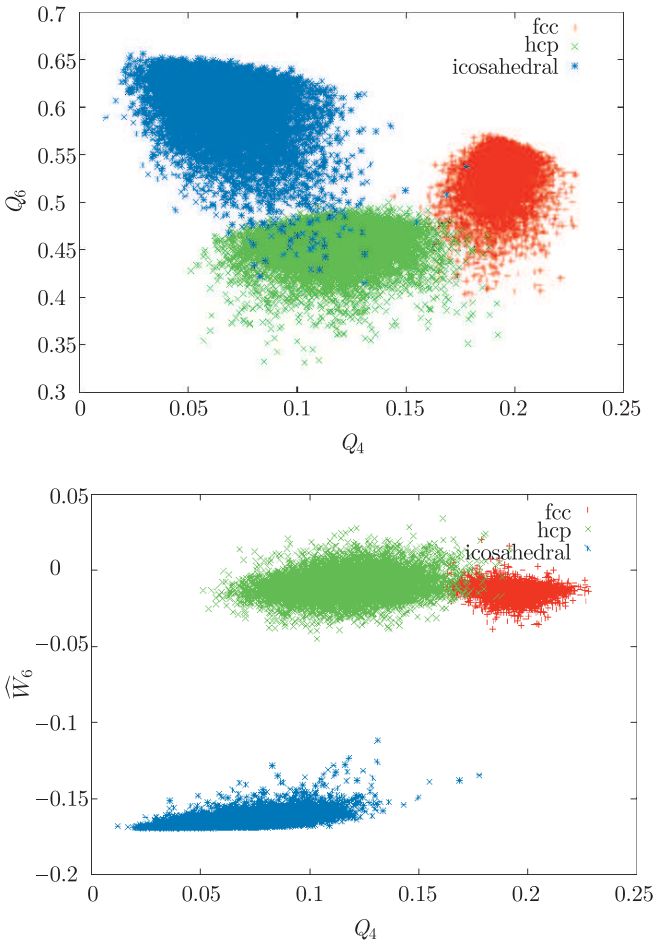

Figure 2. Scatter plots of invariants $Q_4 - Q_6$ (upper plot) and $Q_4 - \widehat{W}_6$ (lower plot) for a central atom of *fcc*, *hcp* and icosahedral clusters

The ranges of Q_4 and $\widehat{W}_6$ which characterise icosahedral, *fcc* and *hcp* clusters were chosen in accordance with the results obtained for disturbed clusters. Table 1 summarises the criteria used to identify the clusters. A cluster was classified as one of the 13-atom structures if the number of nearest neighbours was suitable and the values of chosen BOPs belonged to the defined ranges, otherwise it was classified as a disordered structure.

Table 1. The criteria used to determine the local structure of atoms

Geometry	Q_4 range	$\widehat{W}_6$ range	Number of neighbours
icosahedral	$[-0.01; 0.14]$	$[-0.18; -0.124]$	12
fcc	$[0.153; 0.233]$	$[-0.04; 0.0]$	12
hcp	$[0.043; 0.191]$	$[-0.042; 0.018]$	12
disorder	all other cases		

4. Results

4.1. General structure of the system

The recognition of the structures appearing in the simulations was carried out with the help of the same Winczewski's C++ program as used in the previous section to determine values of BOPs for the model icosahedral, *fcc* and *hcp* clusters.

The starting point of the study was plotting the histograms of selected BOPs averaged over all particles taking part in each simulation. Figure 3 presents their plots for chosen temperatures for the SC, NRL-TB and DCLOTF simulations.

In all cases shaded areas present the ranges which correspond to icosahedral-like structures. It can be observed that in most of the simulations some part of the particles might form the desired structures. Usually, the change of the temperature did not have a big impact on the results. The histograms slightly changed with the rise of the temperature, but the general shape of the plots was similar.

The histograms of $\widehat{W}_6$ parameter obtained from the NRL-TB and DCLOTF simulations resembled ones from the experimental study presented in [6]. The histograms of $\widehat{W}_6$ for the SC simulations at the temperatures of 1200K and higher were slightly shifted towards negative values, *i. e.* the minimal and maximal obtained values were lower and the peak of the histogram appeared at lower value. As a result greater percentage of configurations in the SC simulations were characterised by value of $\widehat{W}_6$ corresponding to icosahedral clusters.

Significantly different results were obtained for the simulations carried out with the SC potential at the temperatures of 1000K and 1100K. What is interesting, the values of BOPs in that cases were concentrated near the points characterising the *fcc* structure (see Table 1). Checking the conditions placed in the mentioned table gave the result that in average about 20% of particles from the simulation at 1000K and 15% of those from the simulation at 1100K displayed the *fcc* symmetry. The number of atoms possessing the *fcc* symmetry, for those two temperatures, was similar during all simulation time. For simulations

of the SC type carried out at the temperatures of 1200K and higher and at all temperatures in the NRL-TB and DCLOTF approaches, less than 1% of all particles were in the *fcc* configuration (Table 2). The number of *hcp* clusters depended on the temperature. The highest number of the structures was detected at the lowest studied temperature and decreased with the rise of the temperature.

Table 2. The average number of *fcc* and *hcp* clusters over the SC, NRL-TB and DCLOTF simulations

Method	Temperature (K)	Average no of *fcc* clusters	Average no of *hcp* clusters
SC	1000	109.5	5.0
SC	1100	73.3	6.0
SC	1200	3.0	5.1
SC	1900	0.2	0.6
NRL-TB	1000	1.0	5.3
NRL-TB	1900	<0.1	0.4
DCLOTF	1000	0.9	5.8
DCLOTF	1900	<0.1	0.4

Such a high percentage of atoms in the *fcc* configuration for particles simulated at the temperature of 1000K and 1100K with SC potential may mean that the simulated copper did not melt. The value of diffusion coefficient confirms this hypothesis, for the 1100K simulations it was equal to $0.04 \cdot 10^{-5} \frac{\mathrm{cm}^2}{\mathrm{s}}$, whereas the molten materials are characterised by the value greater than $1.0 \cdot 10^{-5} \frac{\mathrm{cm}^2}{\mathrm{s}}$. This results are consistent with the properties of copper since those temperatures are below the melting point of copper. The NRL-TB and DCLOTF approaches did not predict it and at the temperatures of 1000K and 1100K simulated molten copper with diffusion coefficient at the temperature of 1100K equal to $2.89 \cdot 10^{-5} \frac{\mathrm{cm}^2}{\mathrm{s}}$ in the NRL-TB simulations and $2.95 \cdot 10^{-5} \frac{\mathrm{cm}^2}{\mathrm{s}}$ in the DCLOTF simulations.

4.2. Icosahedral clusters in the simulations, activation energy of the icosahedral clusters

In almost every simulation some icosahedral clusters were found. Their number was related to the simulation temperature. They were randomly distributed in the simulation box. In the NRL-TB and DCLOTF approaches and in the SC approach at the temperatures 1200K and higher, the number of icosahedral clusters in one frame decreased with the rise of temperature. Furthermore, more frames without any icosahedral clusters appeared. The average number of icosahedral clusters in each simulation is presented in Figure 4.

This results are consistent with the previously mentioned experimental works [6, 7]. The slight differences in range of structures with icosahedral-like symmetry (in the case of the experimental study it was estimated that about 10% of all appearing structures posses icosahedral-like symmetry) may be caused by differences in the definition of what the icosahedral cluster is. The authors of the

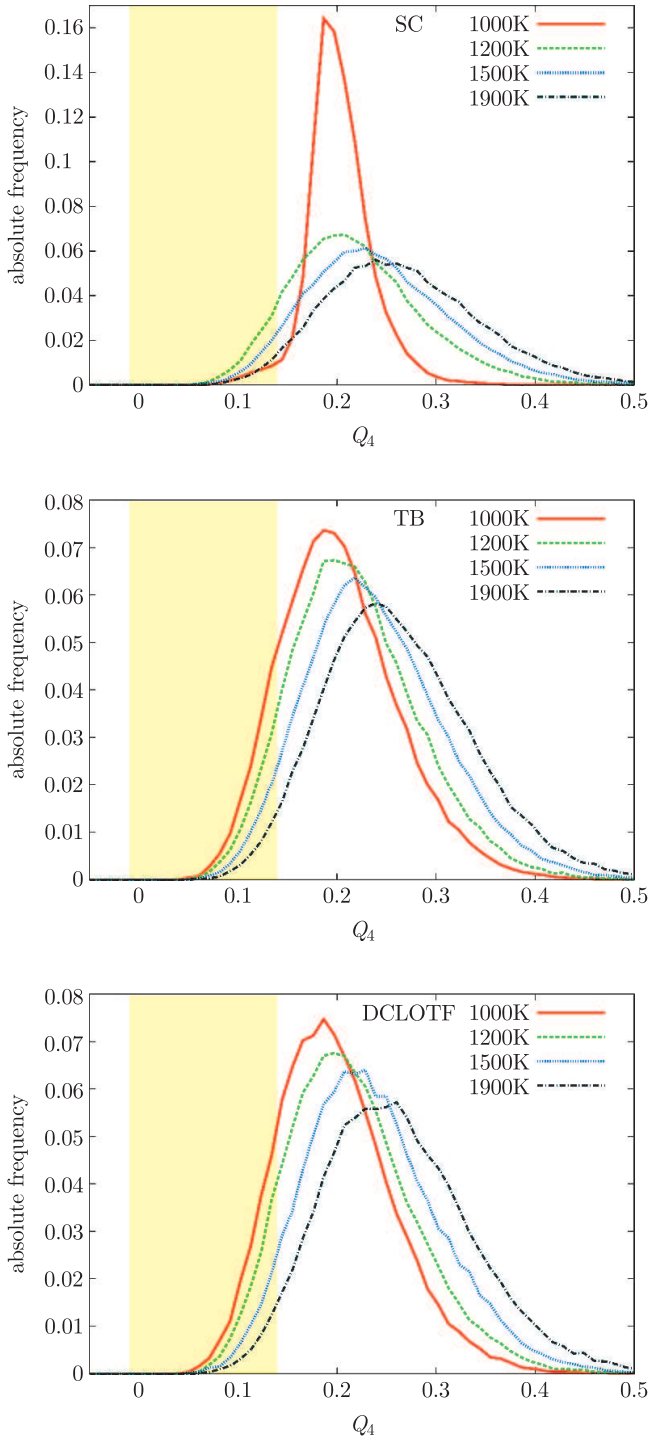

Figure 3. The histograms of Q_4 for particles in the SC, NRL-TB and DCLOTF simulations

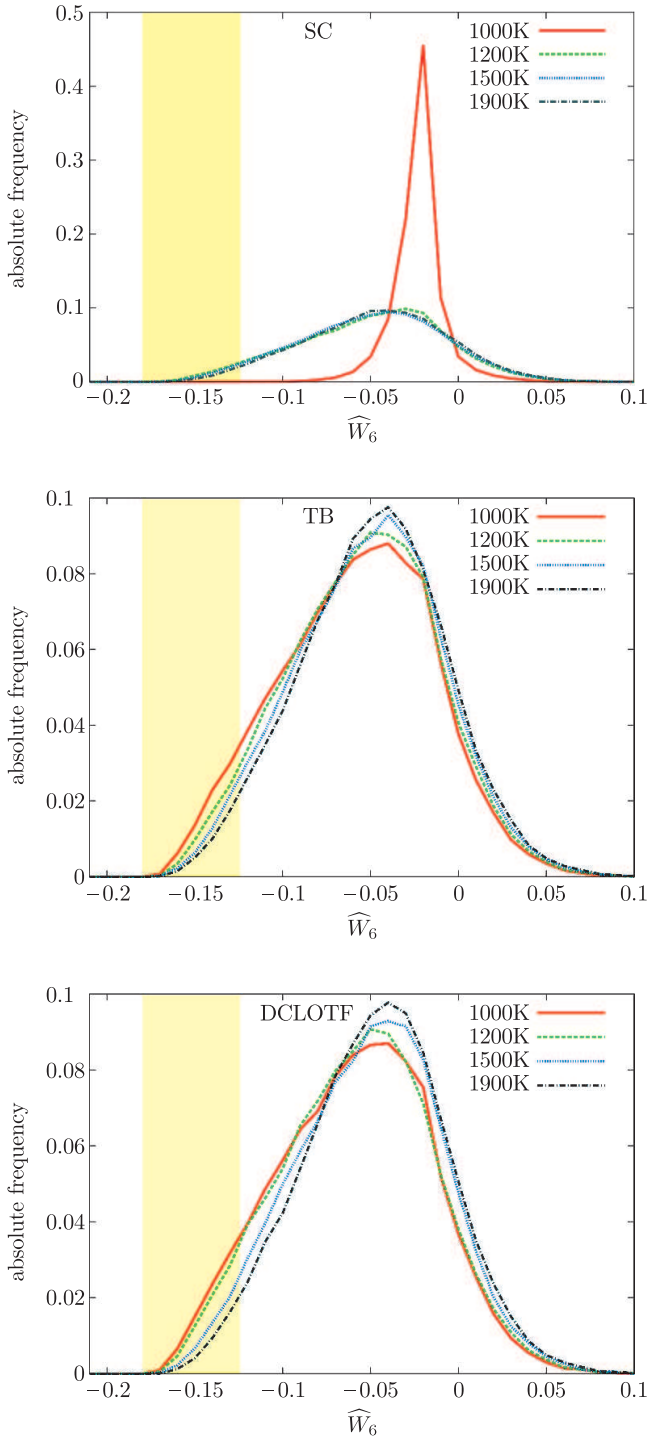

Figure 3 – continued. The histograms of $\widehat{W}_6$ for particles in the SC, NRL-TB and DCLOTF simulations

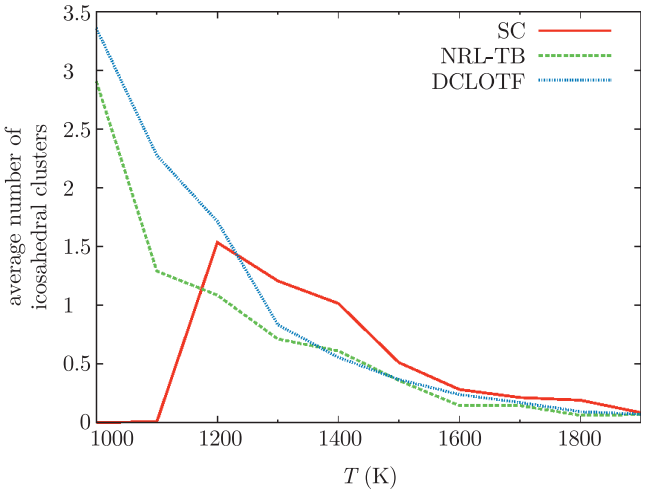

Figure 4. The average number of icosahedral clusters over the SC, NRL-TB and DCLOTF simulations of 500 copper particles

experimental works recognised the clusters with the use of BOPs, although they took into consideration only the $\widehat{W}_6$ invariant, with the range similar to the one used in this study, and did not restrict the number of the nearest neighbours.

Fitting the ratios of average number of atoms in icosahedral configuration ΔN, presented in Figure 4, to the total number of atoms N to the function:

$$\frac{\Delta N}{N} = A \exp\left(-\frac{E_a}{k_B T}\right) \tag{13}$$

gives E_a, the activation energy of icosahedral clusters.

To simplify the calculations, fitting was performed on a logarithmic scale. The above equation was transformed to the form:

$$\ln \Delta N = -\frac{E_a}{k_B} T^{-1} + c \tag{14}$$

where k_B is Boltzmann constant, c is a fitting constant:

$$c = \ln A + \ln N \tag{15}$$

The values of $\ln \Delta N$ as the function of T^{-1} for the SC, NRL-TB and DCLOTF simulations are plotted in Figure 5. The points mark the real values of $\ln \Delta N$ and the lines correspond to the fitted function.

The obtained values of activation energy, together with the values of the constant c, are presented in Table 3.

Table 3. The activation energy of icosahedral clusters and fitting constant c in the SC, NRL-TB and DCLOTF approaches

Method	Activation energy E_a	Fitting constant c
SC	0.81 ± 0.08eV	-7.04 ± 0.63
NRL-TB	0.69 ± 0.06eV	-6.77 ± 0.53
DCLOTF	0.72 ± 0.05eV	-6.75 ± 0.4

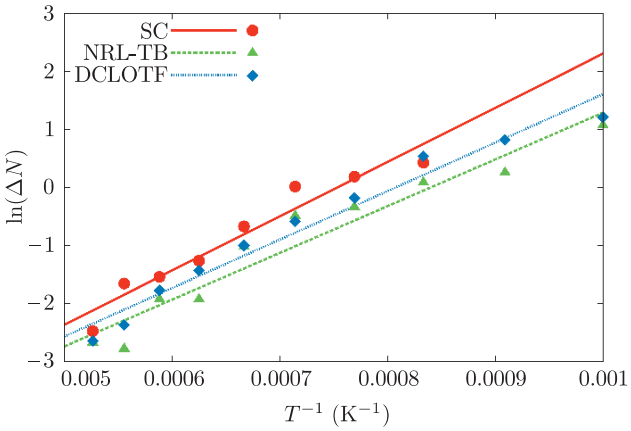

Figure 5. The values of $\ln \Delta N$ as a function of T^{-1} used to calculate the activation energy of icosahedral clusters in the SC, NRL-TB and DCLOTF approaches

4.3. The lifetime of icosahedral clusters

The differences in the average lifetime of icosahedral clusters for various temperatures were rather small. The average lifetime of the structures had a tendency to decrease with the rise of the temperature. The clusters most often existed for 50 fs. The number of longer living structures depended on the temperature, the longest living structures most often appeared in the lowest studied temperatures. In the case of the SC potential the longest living structure appeared at the temperature of 1200 K and lived 450 fs, in the NRL-TB method at 1000 K and lived 300 fs, in DCLOTF method at 1000 K and 1100 K and lived 450 fs. The average lifetime of icosahedral clusters in the SC, NRL-TB and DCLOTF approaches is presented in Figure 6.

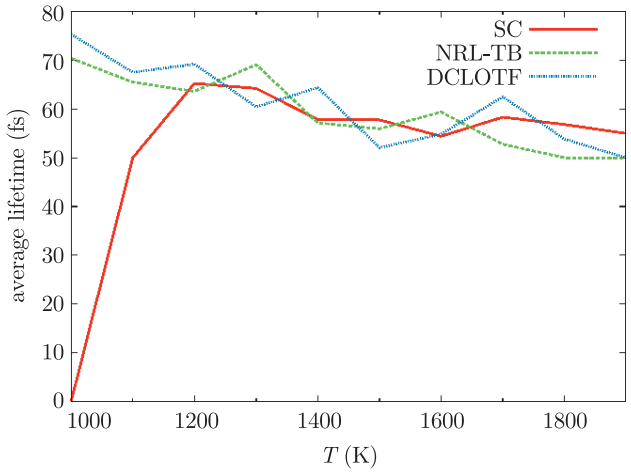

Figure 6. The average lifetime of icosahedral clusters over the SC, NRL-TB and DCLOTF simulations

I found it interesting to investigate the number of icosahedral clusters which did not exist in consecutive frames, but were oscillating around the icosahedral symmetry. The percentage of icosahedral clusters, which were re-formed after less than 500fs of nonexistence, was strongly depending on the temperature. The highest percentage in the NRL-TB and DCLOTF simulations was found at the temperature of 1000K and was equal to 21.6% and 16.4% respectively, in the SC simulations it was equal to 9.1% at 1200K. At the higher of the studied temperatures less icosahedral clusters were re-formed, in all three approaches the percentages significantly decreased with the rise of temperature.

4.4. The correlations between icosahedral clusters

The icosahedral clusters are abhorrent to crystallisation, but they can join. They can correlate in few ways, by sharing one outer atom, an edge (two outer atoms), a face (three outer atoms) or a pentagonal bipyramid (the central atom and six outer atoms). For that reason the data presented in Figure 4 are not equivalent to the number of atoms contributing to the icosahedral clusters, presented in Figure 7.

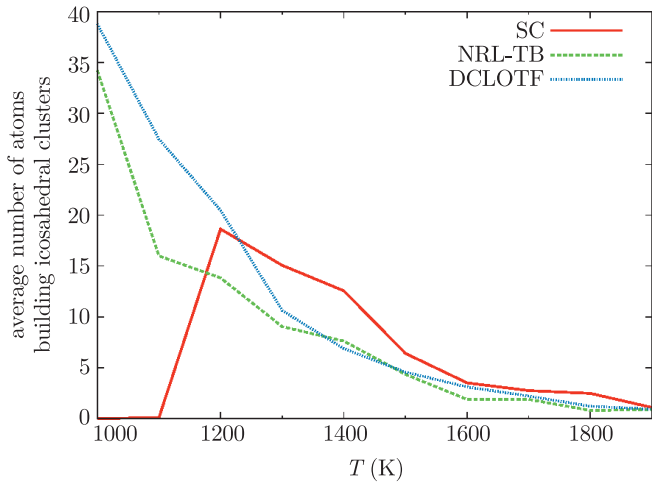

Figure 7. The average number of atoms contributing to icosahedral clusters over the SC, NRL-TB and DCLOTF simulations of 500 copper particles

For atoms simulated with all three approaches, at the temperatures of 1500K and lower, about 90% of the atoms building icosahedral clusters belonged to one cluster. Most of the remaining atoms were building two icosahedral clusters. Some small part of the atoms ($< 1\%$) was contributing to three icosahedral clusters, what was possible since the studied clusters possessed icosahedral-like symmetry, with atoms on disturbed positions.

The correlations between the clusters were studied in the simulations in frames where two or more icosahedral clusters were detected, *i.e.* only in the frames where such correlations were possible. The percentage of icosahedral

clusters which correlate is shown in Table 4. Presented data concerns only the temperatures were the number of the detected icosahedral clusters were significant. It can be observed that the temperature had a weak impact on the correlation of clusters.

Table 4. The percentage of the icosahedral clusters which correlate in the SC, NRL-TB and DCLOTF simulations

Temperature (K)	SC	NRL-TB	DCLOTF
1000	—	44.51%	45.41%
1100	—	33.07%	35.36%
1200	38.04%	15.84%	41.42%
1300	24.56%	20.41%	19.70%
1400	36.84%	42.42%	36.36%
1500	38.46%	58.30%	36.36%

To determine the most often appearing clustering, two kinds of correlations between icosahedral clusters were taken into consideration: the correlations when clusters shared one, two or three outer atoms and the clusters with common pentagonal bipyramid. The results of the investigation, obtained for the temperatures where significant number of clusters correlated, are presented in Table 5. It is clearly noticeable that the correlation where icosahedral clusters share a pentagonal bipyramid was preferable in the three approaches.

Table 5. The distribution by type of clustering in the SC, NRL-TB and DCLOTF simulations

Method	Temperature (K)	Pentagonal bipyramid	Outer atoms
SC	1200	75.2%	24.7%
SC	1300	65.3%	34.7%
SC	1400	84.1%	15.9%
SC	1500	90.8%	9.1%
NRL-TB	1000	84.3%	15.7%
NRL-TB	1100	66.6%	33.4%
NRL-TB	1200	53.0%	47.0%
NRL-TB	1300	87.4%	12.6%
NRL-TB	1400	100.0%	0.0%
NRL-TB	1500	100.0%	0.0%
DCLOTF	1000	74.6%	25.4%
DCLOTF	1100	79.3%	20.7%
DCLOTF	1200	80.6%	19.4%
DCLOTF	1300	39.5%	60.5%
DCLOTF	1400	100.0%	0.0%
DCLOTF	1500	100.0%	0.0%

4.5. The study of incomplete icosahedral clusters

The number of 13-atom icosahedral clusters, even considering clusters with the atoms on disturbed positions, is not significant in close-packed liquids. For that reason I found it interesting to investigate the number of incomplete icosahedral

clusters formed in the simulations. Considered arrangements displayed the lack of one, two or three atoms from the outer shell of the icosahedral cluster. Structures with different degrees of disorder were studied, where position of each atom was changed by randomly generated displacement. The examples of considered configurations are presented in Figure 8.

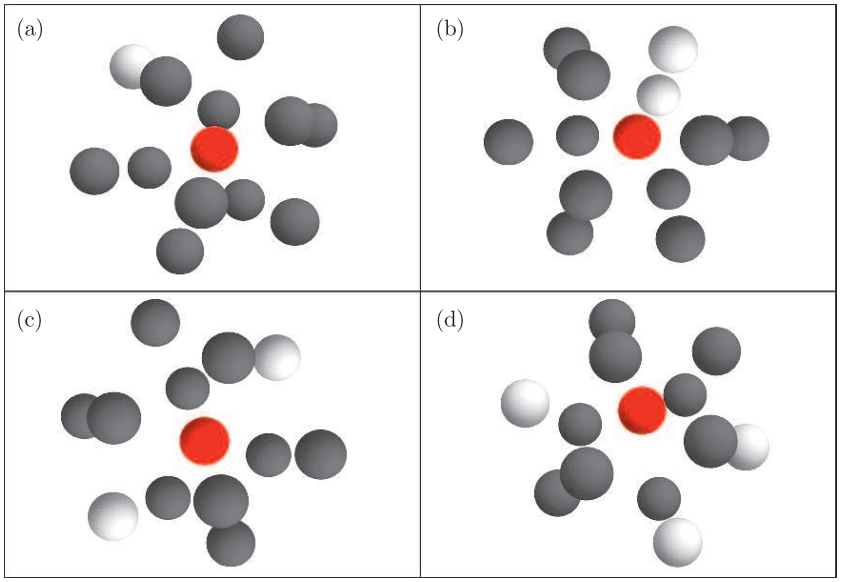

Figure 8. Incomplete icosahedral clusters with lacking atoms (a) 12-atom cluster, (b) and (c) 11-atom clusters, (d) 10-atom cluster

To make the pictures more understandable, in each example the central atom was marked. The atoms missing to form an icosahedral cluster are marked with shaded areas.

Histograms of BOPs for incomplete icosahedral clusters with atoms shifted by a random distance not greater than 5% of the bond length are shown in Figure 9. Values appearing on the histograms, together with the restriction of the number of the nearest neighbours, were used to recognise the types of incomplete icosahedral structures (Table 6).

Table 6. The criteria used to determine the incomplete icosahedral clusters

Type of incomplete icosahedral cluster	Q_4 range	$\widehat{W}_6$ range	Number of neighbours
12-atom	[0.05; 0.19]	[−0.170; −0.13]	11
11-atom	[0.07; 0.27]	[−0.169; −0.12]	10
10-atom	[0.07; 0.30]	[−0.170; −0.11]	9

The average number of incomplete icosahedral clusters over the SC, NRL-TB and DCLOTF simulations (presented in Figure 10) was greater than the average

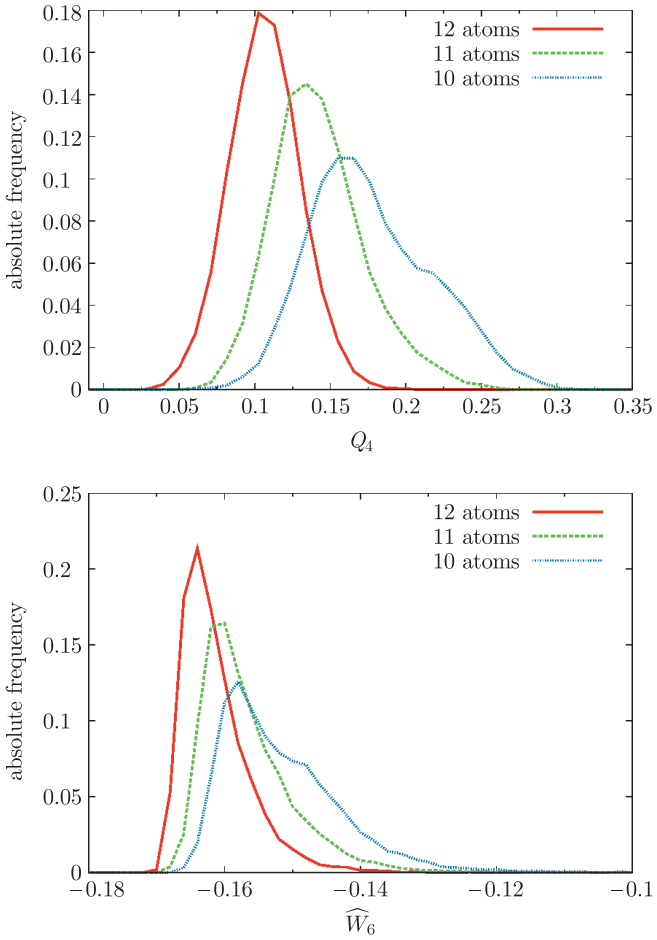

Figure 9. The histograms of parameters Q_4 and $\widehat{W}_6$ for incomplete icosahedral clusters with 5% disorder

number of 13-atom icosahedral clusters (Figure 4). The average number of clusters composed of 12 and 11 atoms decreased with the rise of the temperature in the three approaches. In the simulations of SC type at the temperatures of 1000 K and 1100 K a small number of the clusters was detected.

4.6. The formation and decay of icosahedral clusters

The structures transforming into icosahedral clusters differed for simulations performed at various temperatures. At 1000–1200 K they were usually formed from 12 and 13-atom clusters. What is interesting, those built of twelve atoms in most cases had a form of incomplete icosahedral clusters with one atom removed from the outer shell. Together with the rise of the temperature the percentage of thirteen and twelve atom structures transforming into icosahedral clusters decreased. At the temperature of 1900 K they were the most often formed from eight to eleven atoms.

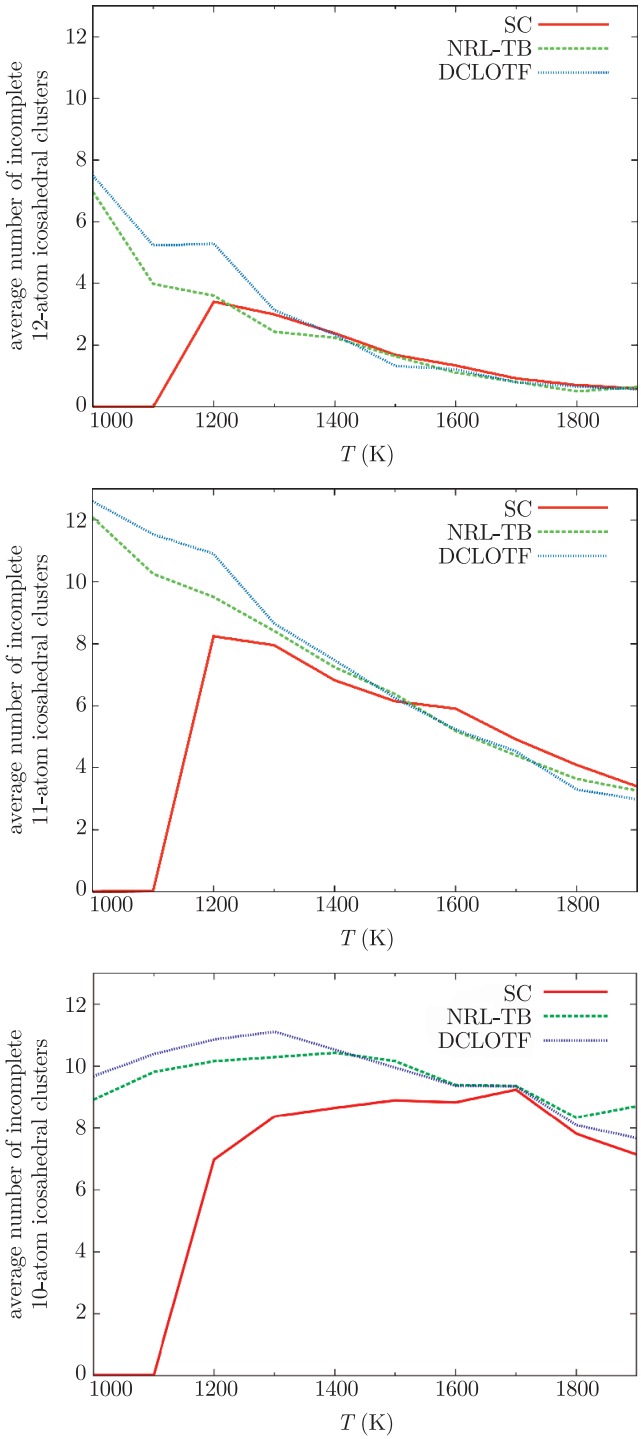

Figure 10. The average number of incomplete 12-atom, 11-atom and 10-atom icosahedral clusters over the SC, NRL-TB and DCLOTF simulations

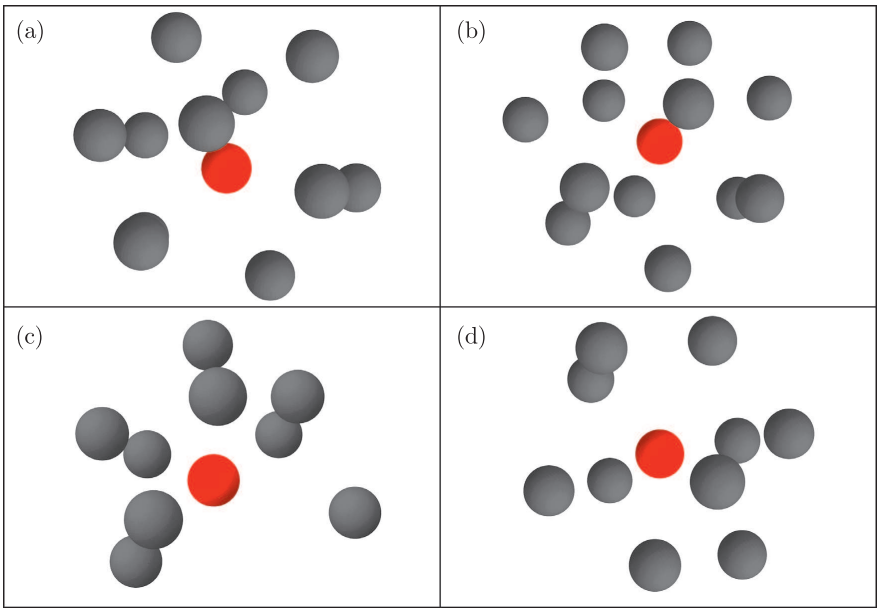

Figure 11. Structures transforming into icosahedral: (a) 12-atom cluster from the NRL-TB simulations at 1000K, (b) 13-atom cluster from the DCLOTF simulations at 1000K, (c) 10-atom cluster from the SC simulation at 1900K, (d) 11-atom cluster from the DCLOTF simulation at 1900K

Table 7. The values of Q_4, $\widehat{W}_6$, number of the nearest neighbours and type of geometry of structures transforming into icosahedral clusters

Case	Q_4	$\widehat{W}_6$	no of nearest neighbours	Geometry
(a) NRL-TB at 1000K	0.111	−0.158	11	12-atom incomplete icosahedral
(b) DCLOTF at 1000K	0.175	−0.0265	12	disorder
(c) SC at 1900K	0.191	−0.132	9	10-atom incomplete icosahedral
(d) DCLOTF at 1900K	0.204	−0.047	10	disorder

The types of structures were similar for the simulations performed in all three approaches. Figure 11 and Table 7 show the examples of configurations transforming into icosahedral clusters. In all four cases the central atom of the cluster was marked. Picture (a) presents a 12-atom incomplete icosahedral cluster, (b) shows a 13-atom disordered cluster, (c) shows the 10-atom incomplete icosahedral cluster and (d) shows a 11-atom disordered cluster.

Usually, the structures resultant from the icosahedral clusters did not have the icosahedral symmetry. The dependence of the number of atoms building them and the temperature was not that clear as in the case of the structures

transforming into icosahedral clusters. However, in most cases, at the highest studied temperatures the structures were containing less atoms than in lower ones.

The examples of structures transforming from icosahedral clusters are presented in Figure 12 and Table 8. They were obtained from the results at various temperatures in the SC, NRL-TB and DCLOTF approaches. All four structures did not posses icosahedral symmetry, although in every case few tetrahedra which formed the clusters could still be noticed.

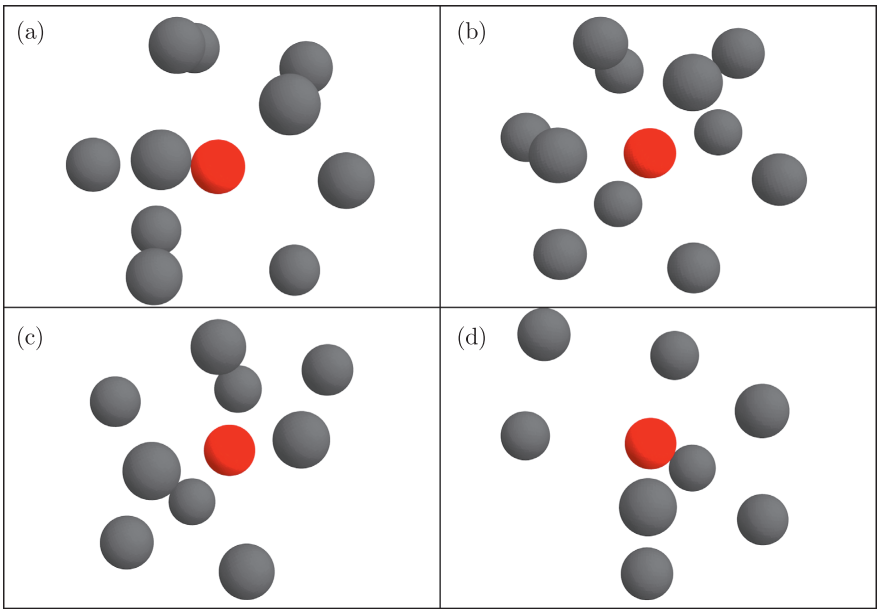

Figure 12. Structures transformed from icosahedral clusters: (a) 11-atom cluster from the DCLOTF simulation at 1000K, (b) 12-atom cluster from the NRL-TB simulation at 1000K, (c) 10-atom cluster from the DCLOTF simulation at 1900K, (d) 9-atom cluster from the SC simulation at 1900K

Table 8. The values of Q_4, $\widehat{W}_6$, number of the nearest neighbours and type of geometry of structures transforming from icosahedral clusters

Case	Q_4	$\widehat{W}_6$	no of nearest neighbours	Geometry
(a) DCLOTF at 1000K	0.201	−0.103	10	disorder
(b) NRL-TB at 1000K	0.152	−0.130	11	disorder
(c) DCLOTF at 1900K	0.217	−0.113	9	disorder
(d) MD at 1900K	0.399	−0.026	8	disorder

5. Conclusions

In this work I used Steinhardt order parameters to study the local geometries in computer-simulated liquid copper. The study used trajectories obtained from simulations performed at ten temperatures between 1000K and 1900 with the use of Sutton-Chen (SC) potential, the Naval Research Laboratory total energy tight-binding (NRL-TB) approach and the divide-and-conquer learn-on-the-fly (DCLOTF) approach. The study was particularly focused on 13-atom icosahedral clusters.

At most of the studied temperatures, the results obtained for the three approaches were similar. The differences occurred at the temperatures of 1000K and 1100K, *i.e.* below the melting point of copper. Only the SC simulations predicted copper not to melt at those temperatures; at both temperatures I detected high number of *fcc* clusters. The NRL-TB approach and the DCLOTF approach (which attempts to mimic the former) incorrectly predicted copper to melt at temperatures that were too low.

At the temperatures of 1200K and higher, the differences between the three approaches were less noticeable. All the three simulations were characterised by a broad range of local geometries, typical for close-packed liquids. The comparison of the histograms of the calculated parameter $\widehat{W}_6$ with experimental data shows that the NRL-TB and DCLOTF approaches better predict the local structure of liquid copper. The values of $\widehat{W}_6$ for the SC calculations were slightly lower, which resulted in a higher number of icosahedral clusters in the simulations compared with experiment.

The average lifetime of icosahedral clusters at each temperature was similar for the three approaches (except for the SC calculations at 1000K and 1100K). Most of the clusters lived for 50fs, which was the shortest considered time. With an increase in temperature the average lifetime of the icosahedral clusters decreased.

In the simulations where more than one icosahedral cluster in a frame were detected, a significant percentage of clusters correlated. In the SC and DCLOTF simulations the percentage of correlating clusters were similar at all investigated temperatures. In the TB simulations the greatest number of clusters correlated at the temperature of 1500K. Most often the clusters correlated by sharing pentagonal bipyramid.

References

[1] Nelson D R 1983 *Phys. Rev. Lett.* **50** 982
[2] Frank F C 1952 *Proc. Royal Soc. London A* **215** 43
[3] Steinhardt P J, Nelson D R and Ronchetti M 1983 *Phys. Rev. B* **28** (2) 784
[4] Landau L D and Lifszyc J M 1978 *Quantum Mechanics*, PWN, Warsaw (in Polish)
[5] Lechner W and Dellago C 2008 *J. Chem. Phys.* **129** 114707
[6] Di Cicco A, Trapananti A, Faggioni S and Filipponi A 2003 *Phys. Rev. Lett.* **91** 135505
[7] Di Cicco A and Trapananti A 2007 *J. Non-Crys. Solids* **353** 3671
[8] Hill T L 1986 *An Introduction to Statistical Thermodynamics*, Dover Publicatios, New York
[9] Dziedzic J 2011 *private communication*

[10] Sutton A P and Chen J 1990 *Philos. Mag. Lett.* **61** 139
[11] Slater J C and Koster G F 1954 *Phys. Rev.* **94**
[12] Mehl M J and Papaconstantopoulos D A 1998 *Topics in Computational Materials Science*, World Scientific Singapore, pp. 169 – 213
[13] Mishin Y, Mehl M J, Papaconstantopoulos D A, Voter A F and Kress J D 2001 *Phys. Rev. B* **63** 224106
[14] Sigalas M and Papaconstantopoulos D A 1994 *Phys. Rev. B* **50** 7255
[15] Dziedzic J, Bobrowski M and Rybicki J 2011 *Phys. Rev. B* **83** 224114
[16] Csányi G, Albaret T, Payne M C and De Vita A 2004 *Phys. Rev. Lett.* **93** 175503
[17] Brillo J and Egry I 2003 *Int. J. Thermophysics* **24** 1155
[18] Dziedzic J 2009 *TASK Quart.* **13** 207
[19] Winczewski S 2011 *private communication*